Hindawi Publishing Corporation
International Journal of Corrosion
Volume 2014, Article ID 565109, 8 pages
http://dx.doi.org/10.1155/2014/565109

Research Article

Effect of C/Si Ratio on the Electrochemical Behavior of a-SiC$_x$:H Coatings on SS301 Substrate Deposited by PECVD

D. Li,[1,2] S. Guruvenket,[2] J. A. Szpunar,[1] and J. E. Klemberg-Sapieha[2]

[1] *Department of Mining and Materials Engineering, McGill University, 3610 University Street, Montreal, QC, Canada H3A 2B2*
[2] *Department of Engineering Physics, Ecole Polytechnique, C.P. 6079, Succ. Centre Ville, Montreal, QC, Canada H3C 3A7*

Correspondence should be addressed to J. E. Klemberg-Sapieha; jsapieha@polymtl.ca

Received 25 November 2013; Revised 19 January 2014; Accepted 20 January 2014; Published 5 March 2014

Academic Editor: Flavio Deflorian

Amorphous hydrogenated silicon carbide (a-SiC$_x$:H) coatings were deposited on stainless steel 301 (SS301) using plasma enhanced chemical vapor deposition with the methane gas flow ranging from 30 to 90 sccm. XRD spectra confirmed the amorphous structure of these coatings. The as-deposited coatings all exhibited homogenous dense feature, and no porosities were observed in SEM and AFM analysis. The a-SiC$_x$:H coatings remarkably increased the corrosion resistance of the SS301 substrate. With the increase of the C concentration, the a-SiC$_x$:H coatings exhibited significantly enhanced electrochemical behavior. The a-SiC$_x$:H coating with the highest carbon concentration acted as an excellent barrier to charge transfer, with a corrosion current of 3.5×10^{-12} A/cm^2 and a breakdown voltage of 1.36 V, compared to 2.5×10^{-8} A/cm^2 and 0.34 V for the SS301 substrate.

1. Introduction

Worldwide demand for stainless steel is rapidly increasing. The combination of high corrosion resistance, low maintenance, and strength makes it a good candidate for various industrial applications [1]. The good corrosion resistance of stainless steel mainly depends on its passivation. The chromium in the alloy forms a self-healing dense oxide layer and prevents the corrosive species from infiltrating into the interior material [2, 3]. However, when stainless steel is exposed to a harsh environment, such as ocean waters or acid rain, the aggressive halide ions (Cl^-, Br^-, I^-, etc.) may penetrate the protective layer and cause a local breakdown of this film [4]. This phenomenon leads to the formation of microgalvanic cells, in which the pits act as the anode and the surrounding intact areas are the cathode, giving rise to the acceleration of the pit growth and chemical dissolution [5–7].

In order to protect the stainless steel against the attack from the aggressive corrosive environment, ceramic coatings are deposited as a protective layer. Silicon carbide (SiC) is known for its outstanding performance in corrosive, erosive, and abrasive media [8, 9]. It has good mechanical properties, low-friction characteristics, and superior corrosion resistance. Over the past years, a number of groups have applied various means to fabricate SiC, for example, reaction-bonded SiC [10], sintered SiC [11–13], and CVD SiC [8, 14–18]. As it stands, CVD SiC exhibits homogenous dense characteristics as well as good adhesion to the metal substrate, making it a better candidate as a protective coating on stainless steel against corrosion.

The crystallinity of CVD SiC relies on the deposition temperature. Liao et al. [19] deposited nanocrystallite β-SiC films by thermal plasma chemical vapor deposition, and they obtained a superhard film with hardness equaling approximately 50 GPa for substrate temperature above 1473 K. Wu et al. [20] investigated corrosion of a three-dimensional SiC/SiC composite with a crystalline CVD SiC coating in environments containing Na_2SO_4 vapor, oxygen, and water vapor at temperatures above 1200 K. They found that the corrosion behavior was greatly related to temperature, and the grain boundaries were severely attacked at temperatures above 1473 K. Barringer et al. [14] studied corrosion of CVD SiC in 773 K supercritical water. They discovered that CVD SiC was preferentially attacked at the grain boundaries. SiC hydrolyzed to hydrated silica species at the surface

Table 1: The deposition conditions of a-SiC_x:H coatings and the corresponding elemental composition, rms roughness, and H/E_r ratios.

Coating	Gas flow (sccm)		Elemental composition (at.%)		C/Si ratio (x)	rms roughness (±0.3 nm)	H/E_r
	CH_4	SiH_4	C	Si			
a-$SiC_{0.59}$:H	30	5	37.2	62.8	0.59	4.3	0.130
a-$SiC_{0.75}$:H	50	5	42.8	57.2	0.75	3.9	0.135
a-$SiC_{0.89}$:H	70	5	47.2	52.8	0.89	4.0	0.142
a-$SiC_{1.02}$:H	90	5	50.5	49.5	1.02	6.1	0.150

and rapidly dissolved into the supercritical water during corrosion.

Amorphous hydrogenated silicon carbide (a-SiC_x:H) can be obtained at much lower temperature (between about 500 and 900 K). Although it has lower hardness (ranging from ~10 to 25 GPa [21]), a-SiC_x:H, like other amorphous alloys, exhibits superior corrosion resistance, thanks to the absence of line and planer defects (e.g., dislocations and grain boundaries) as well as the lack of chemistry inhomogeneity [18].

Although a-SiC_x:H was intensively studied on different aspects, the anticorrosion performance of PECVD a-SiC_x:H coated stainless steel has not been systematically investigated using electrochemical techniques. In this paper, we attempt to explore the electrochemical behavior of the a-SiC_x:H coatings with different C/Si ratio on austenitic stainless steel 301 (SS301) substrate. Various electrochemical properties of these coatings including corrosion current, breakdown voltage, and resistant to charge transfer were examined. Electrochemical impedance spectroscopy (EIS) was conducted to give a direct evaluation on the corrosion resistance of the SS301 substrate and a-SiC_x:H coatings. In addition, wavelength dispersive X-ray spectroscopy (WDS) and atomic force microscopy (AFM) analysis were conducted to establish a good understanding of the all-around properties, as well as their correlation with the electrochemical behaviors of a-SiC_x:H coatings.

2. Experimental

2.1. Coating Deposition. The a-SiC_x:H coatings were deposited on mirror-polished SS301 substrate in a radio frequency (RF, 13.56 MHz) PECVD system. The SS301 substrates, with a dimension of 25 mm × 25 mm × 1 mm, were mechanically polished to a 1 μm rms (root mean square) surface finish, followed by ultrasonic cleaning in acetone and alcohol bath for 10 minutes prior to deposition.

The PECVD chamber was successively evacuated by rotary and turbomolecular pumps to reach a base pressure of 1×10^{-6} Torr. The substrates were then sputtered in argon plasma for 30 minutes under the bias voltage, V_b, of −600 V and the temperature, T_s, of 573 K, in order to remove the surface oxide layer to enhance the adhesion of the coating to the substrate [22]. During deposition, the working pressure, the V_b, and the T_s were maintained at 100 mTorr, −600 V, and 300°C, respectively. The gas flow rate, the corresponding elemental composition, and rms roughness are shown in Table 1. The whole deposition process lasted for 40 min.

2.2. Characterization of the Coatings. Elemental composition of the a-SiC_x:H coatings was determined by wavelength-dispersive spectroscopy (WDS, JXA JEOL-8900L) at the Acc. voltage of 5 kV. Amorphous structure of these coatings was confirmed by grazing incidence X-ray diffraction (XRD) measurements on Rigaku Rotaflex Ru-200B X-ray diffractometer with a Cu X-ray tube at incidence angle of 1.5°.

Field-emission scanning electron microscopy (FESEM, Philips XL30) equipped with an energy dispersive X-ray spectrometry system (EDS) was used to characterize the a-SiC_x:H coatings. The thickness of the coatings was ~2.5 μm as determined by both Sloan Dektak II profilometer measurement and cross-sectional SEM observation.

The morphology and the roughness were measured by means of atomic force microscopy (AFM, Nanoscope III) equipped with an antimony doped Si tip in typing mode, with a scanned area of 3 μm × 3 μm and resolution of 512 × 512.

Mechanical properties, that is, hardness (H) and reduced Young's modulus (E_r), of the coatings were determined by a triboindenter system (Hysitron) equipped with a Berkovich pyramidal tip using the depth sensing indentation technique [23]. For each sample, H and E_r were obtained from at least 25 indentations with peak loads varying from 1 to 5 μN, and the load displacement curves were interpreted using the method proposed by Oliver and Pharr [23].

2.3. Electrochemical Measurements. The electrochemical characterizations were performed at room temperature in a single-compartment electrochemical cell filled with 1 wt. % NaCl electrolyte. A graphitic rod and a standard calomel electrode (SCE) worked as the counter electrode (CE) and the reference electrode (RE), respectively, while the a-SiC_x:H coated SS301 served as the working electrode (WE), with an electrolyte-exposed area of 0.79 cm^2. Autolab PGSTAT302 potentiostat was used to control the potential of the WE as well as to monitor the potential and current *in situ*. The sample was first immersed in the electrolyte for a period of 1 h until the electrode stabilized at open circuit potential (OCP). It was followed by electrochemical impedance spectroscopy (EIS) measurement carried out at OCP with the frequency ranging between 10^5 Hz and 10^{-2} Hz. Afterwards, potentiodynamic polarization experiment was performed by anodically polarizing the working electrode from a potential of −0.2 V up to 2 V with respect to the OCP at a scan rate 5 mV/s. The potential was reversed when a current density of 1×10^{-3} A/cm^2 was reached.

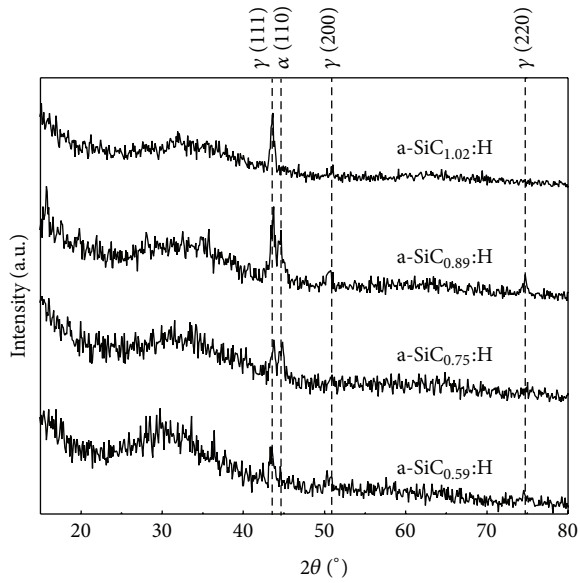

FIGURE 1: XRD spectra of a-SiC_x:H coatings on SS301 substrate.

3. Results and Discussion

3.1. Microstructural and Mechanical Characterization of the a-SiC_x:H Coatings. The evolution of elemental composition measured by WDS as a function of gas flow rate during deposition is summarized in Table 1. As expected, the C/Si ratio continuously increases from 0.59 to 1.02 as the flow of methane increased from 30 to 90 sccm, while the flow of silane was maintained constant at 5 sccm. As assessed using elastic recoil detection in the time-of-flight regime (TOF-ERD), ~25 at. % of hydrogen is present in these a-SiC_x:H films, in agreement with literature values [24].

XRD spectra as shown in Figure 1 confirmed the amorphous structure of the a-SiC_x:H coatings. The peaks in the spectra derived from the austenitic SS301 substrate which consisted of γ and α phase and the corresponding crystallographic planes have been identified as displayed.

Figures 2(a) and 2(b) show the SEM images of the as-deposited a-SiC_x:H coatings of the cross-section and of the surface, respectively. The a-$SiC_{1.02}$:H coating exhibited dense and homogenous featureless microstructure, with no porosity or defect detected as shown in Figure 2(a). The coating possessed good adhesion to the SS301 substrate; there was no delamination or crack at the interface. All the a-SiC_x:H coatings showed similar cross-sectional appearance. The surface morphology of the a-SiC_x:H coatings was investigated by SEM and AFM. As shown in Figure 2(b), the a-$SiC_{0.59}$:H coating had some small particles on the surface, while a-$SiC_{0.75}$:H and a-$SiC_{0.89}$:H coatings were relatively smooth. Unlike the other coatings, a-$SiC_{1.02}$:H coating had a peculiar morphology, showing shallow valleys in the surface. The three-dimensional AFM images as shown in Figure 3 confirmed this observation, and the corresponding rms (root mean square: standard deviation of the height) surface roughness as a function of C/Si ratio is listed in Table 1. The a-$SiC_{0.59}$:H, a-$SiC_{0.75}$:H, and a-$SiC_{0.89}$:H coatings had similar roughness, with the value of ~4 nm, while for the a-$SiC_{1.02}$:H coating, the surface roughness increased to ~6 nm.

The evolution of the mechanical properties, including hardness, H, and reduced Young's modulus, E_r, as a function of the C/Si ratio was displayed in Figure 4. Compared to the SS301 substrate, the a-SiC_x:H coatings substantially enhanced the H from 5 GPa to ~20 GPa and reduced the E_r from 200 GPa to ~150 GPa. Moreover, as the C/Si ratio increased from 0.59 to 1.02, the H and E_r progressively rose from 18 to 23.5 GPa and from 138 to 157 GPa, respectively, which was related to the increase of the C-Si chemical bond fraction. The H/E ratio, as proposed by Leyland and Matthews [25], is a well-accepted indicator to describe and characterize the wear resistance of a material. The a-SiC_x:H coating significantly improved the wear behavior of SS301 [18]. As shown in Table 1, the increase of the H/E_r value from 0.13 to 0.15 with the C/Si ratio will give rise to further enhancement of the tribological properties for the a-SiC_x:H coatings.

3.2. Electrochemical Behavior of the a-SiC_x:H Coatings. In order to investigate the electrochemical behavior of the a-SiC_x:H coatings, potentiodynamic polarization tests were carried out on the a-SiC_x:H coatings as well as on the bare SS301 substrate as a reference; the polarization curves and corresponding results are displayed in Figures 5 and 6, respectively. The pitting resistance is reflected by the breakdown voltage, E_{BD}, at which the penetration of Cl^- ions through the microdefects in the protective layer gives rise to a sharp current increase as shown in the polarization curves [4].

All the a-SiC_x:H coatings substantially improved the corrosion resistance of the SS301 substrate; the corrosion current, i_{corr}, was decreased by more than two orders of magnitude, and the E_{BD} was raised at the same time. Moreover, as the C concentration increases, the corrosion resistance of the a-SiC_x:H coatings is significantly enhanced, in terms of both the reduction of the i_{corr} and the increase of the E_{BD} in synergy. In particular, the a-$SiC_{1.02}$:H coating possessed the lowest i_{corr} (3.5×10^{-12} A/cm^2) and the highest E_{BD} (1.36 V). It exhibited a wide range of passivation region and retained the current density at a low value (below 10^{-10} A/cm^2) until a high E_{BD} was reached. Such a phenomenon indicated that this coating served as an excellent barrier against electrochemical reactions.

In order to obtain more insight into the general corrosion behavior of the a-SiC_x:H coatings with different C concentration, the EIS test results were analyzed and compared. Nyquist plots were adopted to present the EIS data and the spectra fitting was performed using proper equivalent circuits. The basic circuit, Randles circuit, was used to interpret the EIS spectra of the bare SS301 substrate. As shown in Figure 7(a), it consists of solution resistance, R_s, in series with a parallel combination of a constant phase element (CPE) corresponding to the double layer capacitor, Q_{dl}, and a charge transfer resistance, R_{ct}. The Q_{dl} forms at the interface between the electrode and its surrounding electrolyte, as ions from the solution, are attracted to the electrode surface, resulting in

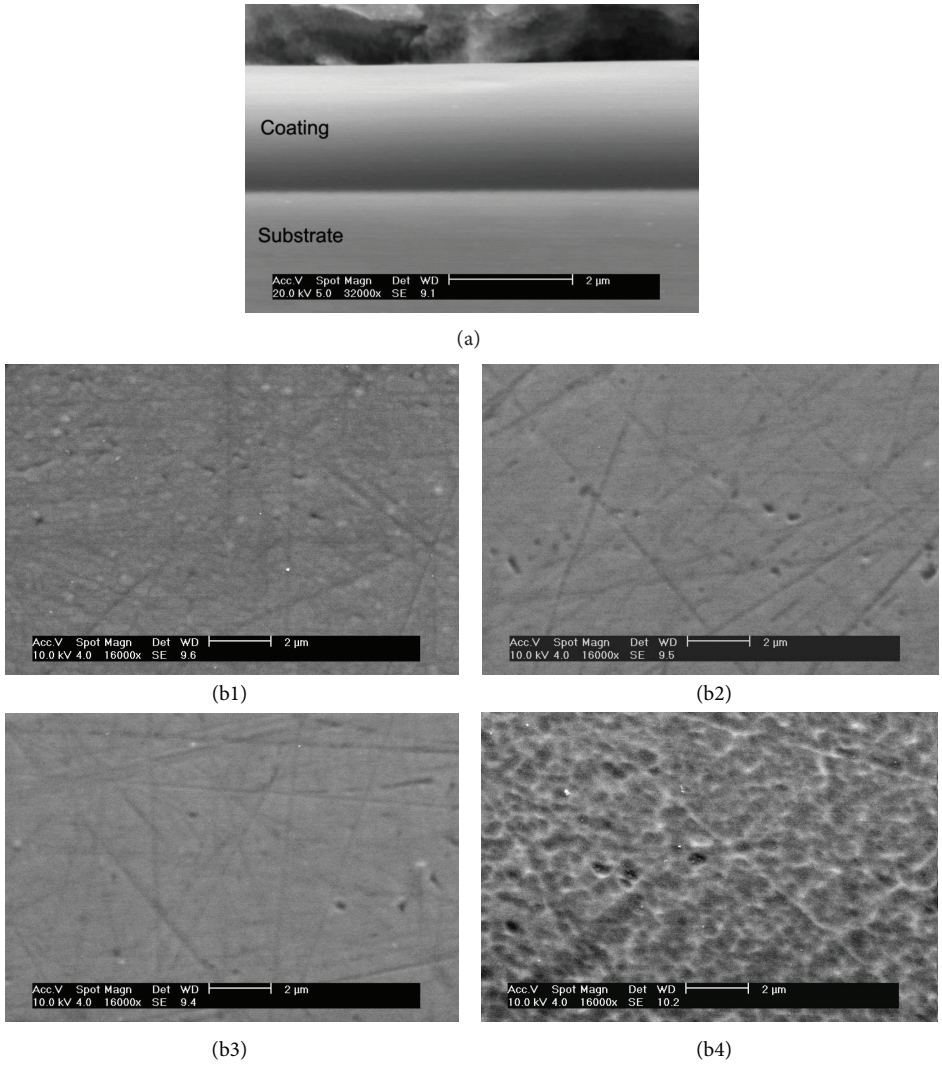

Figure 2: (a) Cross-sectional SEM image of a-$SiC_{1.02}$:H coating; (b) SEM images of (b1) a-$SiC_{0.59}$:H, (b2) a-$SiC_{0.75}$:H, (b3) a-$SiC_{0.89}$:H, and (b4) a-$SiC_{1.02}$:H coatings.

charge buildup at the interface. Its impedance is expressed in the following form:

$$Z_Q = \frac{1}{\left[Y_0(j\omega)^n\right]}, \quad (1)$$

where ω is the angular frequency, Y_0 is a constant of Q_{dl}, and n is an empirical exponent of Q_{dl} [26], which represents the deviation of the impedance from the pure capacitor behavior resulting from the inhomogeneity in the coating system [27].

The a-SiC_x:H coatings exhibited a more complex electrochemical behavior; therefore, the equivalent circuit as shown in Figure 7(b) was employed to interpret their impedance spectra. It consists of the following components: R_s—the solution resistance; Q_f—CPE corresponding to the capacitance of the intact coating; R_p—solution resistance inside the pores; R_{ct}—the resistance to charge transfer; and Q_{dl}—CPE corresponding to the double layer capacitance in the pit at the interface between the solution and the sample.

As displayed in the Nyquist plot (Figure 7(c)), the best-fit curves (solid lines) represent the experimental data (dotted lines) very well. The results derived from the spectra modeling are listed in Table 2, and particularly, the R_{ct}, which is reversely proportional to the corrosion rate, is compared in Figure 8. Compared to the bare SS301 (R_{ct} = 1.37 MΩ), all the a-SiC_x:H coatings substantially enhanced the corrosion resistance. Moreover, the R_{ct} significantly rose from 299 MΩ to 10.5 GΩ, as the C/Si ratio increased from 0.59 to 1.02. This observation is in good agreement with the previous potentiodynamic polarization test; the coating with a high R_{ct} exhibited a low i_{corr}.

Such a significant improvement of the electrochemical properties of the a-SiC_x:H coatings can be attributed to the increase of Si–C and C–C bonds and the decrease of Si-Si

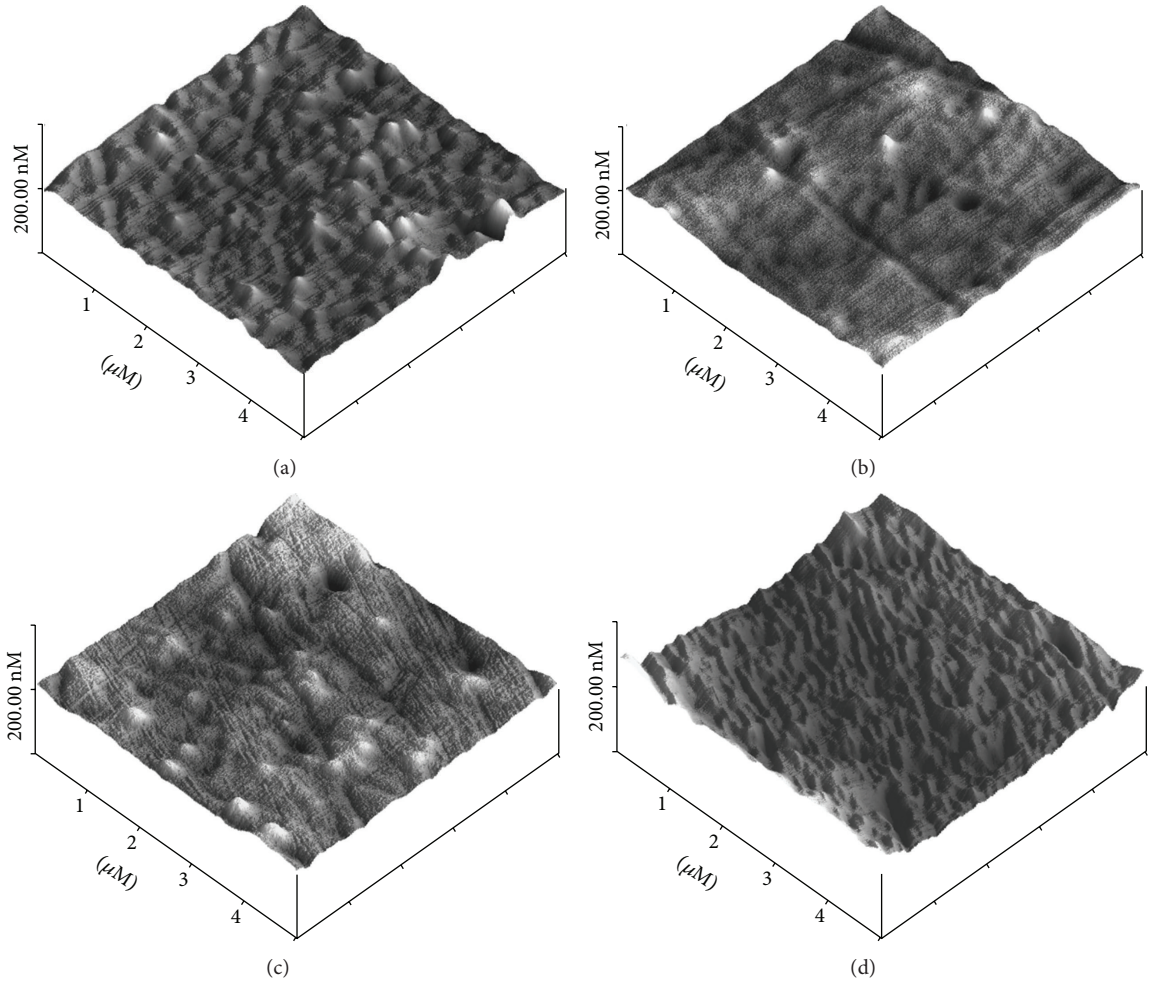

FIGURE 3: Three-dimensional AFM images of (a) a-$SiC_{0.59}$:H, (b) a-$SiC_{0.75}$:H, (c) a-$SiC_{0.89}$:H, and (d) a-$SiC_{1.02}$:H coatings on SS301 substrate.

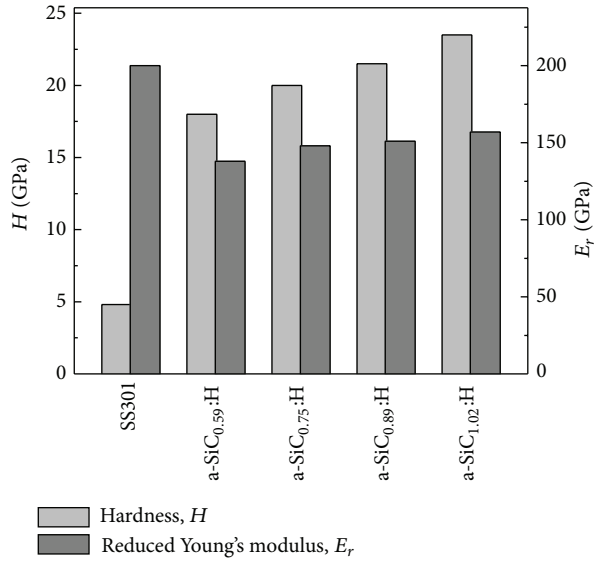

FIGURE 4: Mechanical properties of a-SiC_x:H coatings.

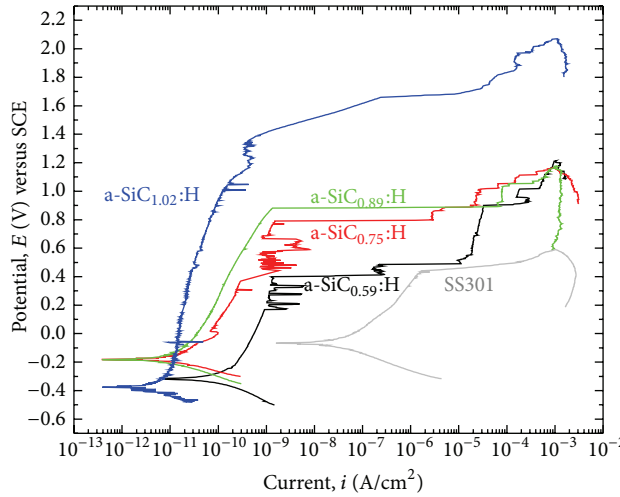

Figure 5: Potentiodynamic polarization curves of a-SiC$_x$:H coatings and SS301 substrate.

Table 2: The best-fit values of EIS spectra of SS301 and a-SiC$_x$:H samples.

Sample	R_s (Ω cm^2)	$Q_f(Y_0)$ (F/cm^2)	$Q_f(n)$	R_p (Ω cm^2)	$Q_{dl}(Y_0)$ (F/cm^2)	$Q_{dl}(n)$	R_{ct} (Ω cm^2)
SS301	57	—	—	—	2.8×10^{-5}	0.907	1.37×10^{6}
a-SiC$_{0.59}$:H	44	5.1×10^{-9}	0.962	8.84×10^{4}	1.0×10^{-8}	0.593	2.99×10^{8}
a-SiC$_{0.75}$:H	42	6.6×10^{-9}	0.966	1.29×10^{5}	6.7×10^{-8}	0.613	2.19×10^{9}
a-SiC$_{0.89}$:H	51	6.8×10^{-9}	0.946	5.36×10^{8}	2.2×10^{-9}	0.608	3.35×10^{9}
a-SiC$_{1.02}$:H	46	9.7×10^{-11}	0.991	2.69×10^{9}	7.0×10^{-11}	0.506	1.05×10^{10}

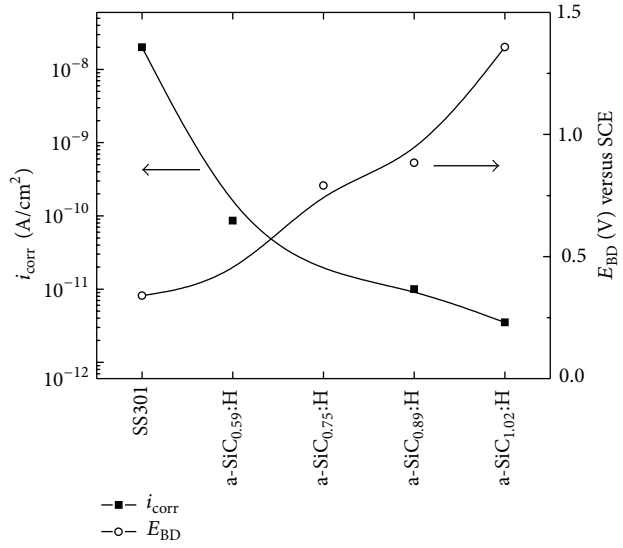

Figure 6: i_{corr} and E_{BD} derived from the potentiodynamic polarization curves.

bonds in synergy as more C incorporates into the coatings. The Si-rich a-SiC$_x$:H mainly consists of a-Si:H and a-SiC:H phases [28]. With the increase of C concentration, the a-Si:H phase gradually diminishes [29]. The principal corrosion reaction in SiC involves dissolution of Si [30], and hence such a decrease of Si concentration and increase of inert a-SiC:H give rise to the enhanced anticorrosion properties. The a-SiC$_{1.02}$:H coating, with a 1 : 1 stoichiometric C/Si ratio, exhibits superior corrosion performance by acting as an excellent barrier against charge transfer.

4. Conclusions

The corrosion properties of a-SiC$_x$:H coatings with different C concentration have been investigated using electrochemical techniques, and the conclusions are made as follows.

(1) The a-SiC$_x$:H coatings possess homogeneous dense microstructure. With the increase of the CH_4 gas flow from 30 to 90 sccm during deposition, the C/Si ratio progressively increases from 0.59 to 1.02.

(2) The a-SiC$_x$:H coatings exhibit superior mechanical and electrochemical properties compared with SS301. The increase of the C concentration leads to simultaneous further enhancement of the mechanical and electrochemical properties of the a-SiC$_x$:H coatings.

(3) The a-SiC$_{1.02}$:H coating, with a 1 : 1 stoichiometric C/Si ratio, exhibits superior corrosion performance by acting as an excellent barrier against charge transfer, showing a corrosion current of 3.5×10^{-12} A/cm^2 and a breakdown voltage of 1.36 V, compared to 2.5×10^{-8} A/cm^2 and 0.34 V for the SS301 substrate.

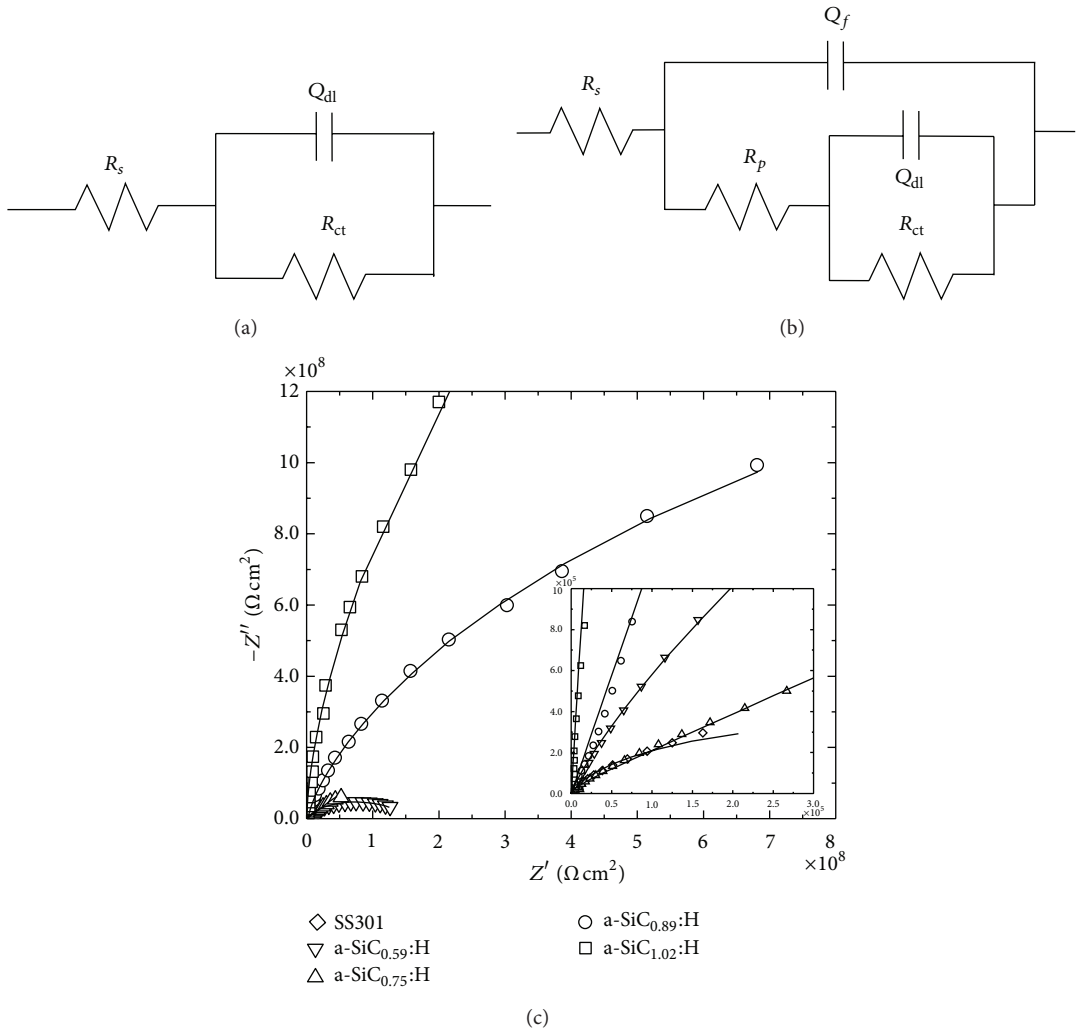

Figure 7: Equivalent circuits used for (a), (b) the EIS spectra fitting, and (c) Nyquist plot of EIS spectra for the a-SiC$_x$:H coatings and for the bare SS301 substrate.

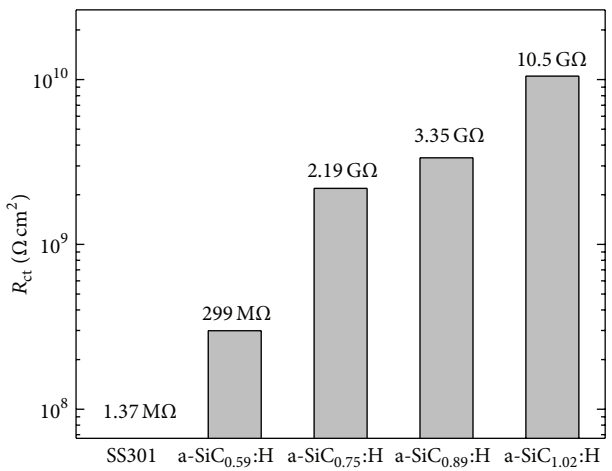

Figure 8: Resistance to charge transfer of the bare SS301 substrate and the a-SiC$_x$:H coatings with different C contents.

Conflict of Interests

The authors declare that there is no conflict of interests regarding the publication of this paper.

Acknowledgments

The authors are thankful for the financial support by NSERC and CRIAQ within the CRDPJ328038-05 Project.

References

[1] S. Lamb, CASTI Publishing Inc./ASM International, Quebec, Canada, 2001.

[2] Y.-J. Kim, "Analysis of oxide film formed on type 304 stainless steel in 288°C water containing oxygen, hydrogen, and hydrogen peroxide," *Corrosion*, vol. 55, no. 1, pp. 81–88, 1999.

[3] N. Sato, "An overview on the passivity of metals," *Corrosion Science*, vol. 31, pp. 1–19, 1990.

[4] S. Ningshen, U. Kamachi Mudali, V. K. Mittal, and H. S. Khatak, "Semiconducting and passive film properties of nitrogen-containing type 316LN stainless steels," *Corrosion Science*, vol. 49, no. 2, pp. 481–496, 2007.

[5] E. Stansbury and R. Buchanan, *Fundamentals of Electrochemical Corrosion*, ASM International, 2000.

[6] N. Sato, "A theory for breakdown of anodic oxide films on metals," *Electrochimica Acta*, vol. 16, no. 10, pp. 1683–1692, 1971.

[7] D. A. Jones, *Principles and Prevention of Corrosion*, Macmillan, 1991.

[8] C. R. Stoldt, M. C. Fritz, C. Carraro, and R. Maboudian, "Micromechanical properties of silicon-carbide thin films deposited using single-source chemical-vapor deposition," *Applied Physics Letters*, vol. 79, no. 3, pp. 347–349, 2001.

[9] M. Azzi, M. Paquette, J. E. Klemberg-Sapieha, and L. Martinu, in *Proceedings of the 52th Annual SVC Conference*, Santa-Clara, Calif, USA, May 2009.

[10] W.-J. Kim, H. S. Hwang, and J. Y. Park, "Corrosion behavior of reaction-bonded silicon carbide ceramics in high-temperature water," *Journal of Materials Science Letters*, vol. 21, no. 9, pp. 733–735, 2002.

[11] V. Presser, O. Krummhauer, K. G. Nickel, A. Kailer, C. Berthold, and C. Raisch, "Tribological and hydrothermal behaviour of silicon carbide under water lubrication," *Wear*, vol. 266, no. 7-8, pp. 771–781, 2009.

[12] S. Somiya, "Hydrothermal corrosion of nitride and carbide of silicon," *Materials Chemistry and Physics*, vol. 67, no. 1–3, pp. 157–164, 2001.

[13] A. Andrews, M. Herrmann, M. Sephton, C. Machio, and A. Michaelis, "Electrochemical corrosion of solid and liquid phase sintered silicon carbide in acidic and alkaline environments," *Journal of the European Ceramic Society*, vol. 27, no. 5, pp. 2127–2135, 2007.

[14] E. Barringer, Z. Faiztompkins, H. Feinroth et al., "Corrosion of CVP silicon carbide in 500°C supercritical water," *Journal of the American Ceramic Society*, vol. 90, no. 1, pp. 315–318, 2007.

[15] C. J. Jensen and W. K. S. Chiu, "Open-air laser-induced chemical vapor deposition of silicon carbide coatings," *Surface and Coatings Technology*, vol. 201, no. 6, pp. 2822–2828, 2006.

[16] L. Zambov, K. Weidner, V. Shamamian et al., "Advanced chemical vapor deposition silicon carbide barrier technology for ultralow permeability applications," *Journal of Vacuum Science and Technology A*, vol. 24, no. 5, pp. 1706–1713, 2006.

[17] T. Goto, H. Homma, and T. Hirai, "Effect of oxygen partial pressure on the high-temperature oxidation of CVD SiC," *Corrosion Science*, vol. 44, no. 2, pp. 359–370, 2002.

[18] D. Li, S. Guruvenket, M. Azzi, J. A. Szpunar, J. E. Klemberg-Sapieha, and L. Martinu, "Corrosion and tribo-corrosion behavior of a-SiC_x:H, a-SiN_x:H and a-SiC_xN_y:H coatings on SS301 substrate," *Surface and Coatings Technology*, vol. 204, no. 9-10, pp. 1616–1622, 2010.

[19] F. Liao, S. L. Girshick, W. M. Mook, W. W. Gerberich, and M. R. Zachariah, "Superhard nanocrystalline silicon carbide films," *Applied Physics Letters*, vol. 86, no. 17, Article ID 171913, pp. 1–3, 2005.

[20] S. Wu, L. Cheng, L. Zhang, Y. Xu, X. Luan, and H. Mei, "Corrosion of SiC/SiC composite in Na_2SO_4 vapor environments from 1000 to 1500°C," *Composites A*, vol. 37, no. 9, pp. 1396–1401, 2006.

[21] J. F. Zhao, P. Lemoine, Z. H. Liu, J. P. Quinn, P. Maguire, and J. A. McLaughlin, "A study of microstructure and nanomechanical properties of silicon incorporated DLC films deposited on silicon substrates," *Diamond and Related Materials*, vol. 10, no. 3–7, pp. 1070–1075, 2001.

[22] E. Angelini, S. Grassini, F. Rosalbino, F. Fracassi, and R. D'Agostino, "Electrochemical impedance spectroscopy evaluation of the corrosion behaviour of Mg alloy coated with PECVD organosilicon thin film," *Progress in Organic Coatings*, vol. 46, no. 2, pp. 107–111, 2003.

[23] W. C. Oliver and G. M. Pharr, "Improved technique for determining hardness and elastic modulus using load and displacement sensing indentation experiments," *Journal of Materials Research*, vol. 7, no. 6, pp. 1564–1580, 1992.

[24] D. Brassard and M. A. El Khakani, "Dielectric properties of amorphous hydrogenated silicon carbide thin films grown by plasma-enhanced chemical vapor deposition," *Journal of Applied Physics*, vol. 93, no. 7, pp. 4066–4071, 2003.

[25] A. Leyland and A. Matthews, "On the significance of the H/E ratio in wear control: a nanocomposite coating approach to optimised tribological behaviour," *Wear*, vol. 246, no. 1-2, pp. 1–11, 2000.

[26] Z. Bou-Saleh, A. Shahryari, and S. Omanovic, "Enhancement of corrosion resistance of a biomedical grade 316LVM stainless steel by potentiodynamic cyclic polarization," *Thin Solid Films*, vol. 515, no. 11, pp. 4727–4737, 2007.

[27] H.-G. Kim, S.-H. Ahn, J.-G. Kim, S. J. Park, and K.-R. Lee, "Electrochemical behavior of diamond-like carbon films for biomedical applications," *Thin Solid Films*, vol. 475, no. 1-2, pp. 291–297, 2005.

[28] B. Racine, A. C. Ferrari, N. A. Morrison, I. Hutchings, W. I. Milne, and J. Robertson, "Properties of amorphous carbon-silicon alloys deposited by a high plasma density source," *Journal of Applied Physics*, vol. 90, no. 10, pp. 5002–5012, 2001.

[29] S. Guruvenket, M. Azzi, D. Li, J. A. Szpunar, L. Martinu, and J. E. Klemberg-Sapieha, "Structural, mechanical, tribological, and corrosion properties of a-SiC:H coatings prepared by PECVD," *Surface and Coatings Technology*, vol. 204, no. 21-22, pp. 3358–3365, 2010.

[30] R. Divakar, S. G. Seshadri, and M. Srinivasan, "Electrochemical techniques for corrosion rate determination in ceramics," *Journal of the American Ceramic Society*, vol. 72, no. 5, pp. 780–784, 1989.